

**SPATIAL FILTERS FOR LINEARLY POLARIZED
ANTENNAS USING FREE STANDING FREQUENCY
SELECTIVE SURFACE**

A. E. Farahat and K. F. A. Hussein

Microwave Engineering Department
Electronics Research Institute
Dokki, Cairo, Egypt

N. M. El-Minyawi

Faculty of Engineering
Ain Shams University
Cairo, Egypt

Abstract—Free standing planar frequency selective surfaces (FSSs) are studied when utilized as spatial filters for linearly polarized antennas. The antenna spatial filter investigated in the present work is constructed up as a finite planar array of conducting strip dipoles. The electric field integral equation (EFIE) technique with the Rao-Wilton-Glison (RWG) basis functions are used to get the current distribution on the conducting strips. The current distribution and backscattered electric field due to an incident plane wave are calculated and compared to some published work. The effect of polarization on the scattered field, and the frequency response of the spatial filter are studied. To test the operation of the proposed planar FSS, a bowtie antenna is used with the FSS employed as a spatial filter. The field transmitted by the antenna and passed over a wide frequency band through the FSS is calculated. It is shown that such a free standing planar FSS can operate as a band stop filter for linearly polarized antennas. It is also shown that even when the size of the array is reduced, the FSS maintains its frequency response with a very slight change in the center frequency of the stop band. The effect of element size, spacing between the elements, and interleaving the columns of the FSS on the frequency response of the FSS are studied. The effect of the spatial filter on the antenna input impedance is studied over a wide frequency band. The radiation pattern of the bowtie is calculated in the presence

of the spatial filter. It is shown that the existence of the later causes considerable reduction in the radiation pattern within the stop band of the filter.

1. INTRODUCTION

Frequency selective surfaces are periodic structures in either one or two dimensions (i.e., singly or doubly periodic structures) which performs a spatial filter operation. Thus, depending on their physical construction, material and geometry, they are divided into low-pass, high-pass, band-pass and band-stop filters. FSSs consist of elements arranged in a planar or curved periodic array of single or multiple layers to create a specific filter response. The properties of the filter can be varied by choosing the appropriate element type, dimensions, volumetric structure, and spacing between the elements. Early work was concerned with the use of FSS in Cassegrainian subreflectors in parabolic dish antennas [1]. FSSs are now employed in terrestrial and airborne radomes [2]. Radomes with finite curved frequency selective surfaces comprised of conformal antenna arrays have been introduced in [15]. Also, FSSs have been used in electromagnetic shielding applications [3, 4]. In the near infrared and visible portion of the spectrum, periodic screens have been proposed as spatial filters [5].

There are many techniques used for the analysis and design of FSS. The most common is the modal (spectral domain) analysis [6] in which the distribution of current induced in conducting elements (or fields in slots) is represented as a series of suitable basis functions. Local fields are expanded as a set of Floquet modes [7, 8]. This technique assumes that the array has infinite dimensions, but if the array is finite, special assumptions and approximations should be applied to handle the array truncation [7]. Multi-band frequency selective surfaces have found many applications in microwave and optical communication systems. Many techniques have been proposed for the analysis and design of the employed FSSs [16–20]. In order to model the finite array FSS accurately, a numerical technique should be used that simulate the whole array. In the present work, the method of moment (MoM) solution of the spatial domain EFIE is applied to analyze planar FSS of finite extension. Studying the FSS problem in the spatial domain will enable us to study the mutual effects between an FSS and an antenna put near to it. This was not feasible in the spectral domain methods as the existence of the antenna in the vicinity of the FSS spoils the spatial periodicity of the structure and hence invalidates the spectral domain treatment. The disadvantages of doing this are the requirement for

large computer storage and long simulation time that will increase by increasing the size of the FSS.

The EFIE technique for scattering from conducting surfaces of arbitrary shape was developed by Rao, Wilton and Glisson in [9], where triangular basis functions, commonly known as RWG basis functions, are introduced for current expansion on the conducting surface. In the present work, the EFIE technique employing triangular patches model for the conducting surfaces and RWG basis function for the surface current expansion is used to study the characteristics of an array of strip dipoles arranged in planar configuration to be used as a spatial filter for linearly polarized antennas.

2. APPLICATION OF THE EFIE TECHNIQUE AND CALCULATION OF THE SCATTERED FIELD

In the present analysis, the EFIE approach described in [9] is applied. The electric field radiated due to a surface charge density σ and current \mathbf{J} flowing on a conducting surface, S , can be obtained by the following expression,

$$\mathbf{E}^s(\mathbf{r}) = -j\omega\mathbf{A}(\mathbf{r}) - \nabla\Phi(\mathbf{r}) \quad (1)$$

where $\mathbf{A}(\mathbf{r})$ is the magnetic vector potential defined as,

$$\mathbf{A}(\mathbf{r}) = \frac{\mu}{4\pi} \int_{S'} \mathbf{J} \frac{e^{-jk|\mathbf{r}-\mathbf{r}'|}}{|\mathbf{r}-\mathbf{r}'|} dS' \quad (2)$$

and $\Phi(\mathbf{r})$ is the electric scalar potential defined as,

$$\Phi(\mathbf{r}) = \frac{1}{4\pi\epsilon} \int_{S'} \sigma \frac{e^{-jk|\mathbf{r}-\mathbf{r}'|}}{|\mathbf{r}-\mathbf{r}'|} dS' \quad (3)$$

where \mathbf{r}' is a point on S and \mathbf{r} is a point in free space. The surface charge density σ is related to the surface divergence of the current \mathbf{J} flowing on S through the equation of continuity,

$$\nabla_s \cdot \mathbf{J} = -j\omega\sigma \quad (4)$$

We derive an integrodifferential equation for \mathbf{J} by enforcing the boundary condition $\hat{\mathbf{n}} \times (\mathbf{E}^i + \mathbf{E}^s) = 0$ on S to obtain,

$$-\mathbf{E}_{\text{tan}}^i(\mathbf{r}) = [-j\omega\mathbf{A}(\mathbf{r}) - \nabla\Phi(\mathbf{r})]_{\text{tan}} \quad (5)$$

The surface is divided into a number of triangular patches. Each patch has three edges; an edge which belongs to only one triangular patch is

called a *boundary edge*. Such an edge exists only on the rim of an open surface and hence, it has no electric current component flowing normal to it. As shown in Figure 1, an edge which belongs to two adjacent triangular patches is called a *non-boundary edge*. Only non-boundary edges can have electric current components flowing normal to them.

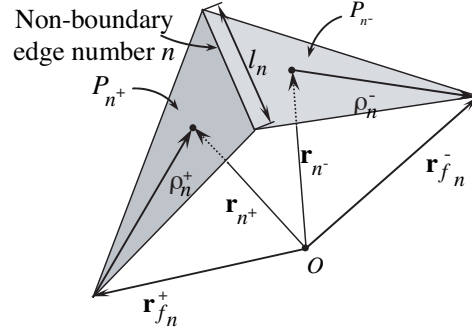


Figure 1. Triangular-patch model for surfaces of arbitrarily-shaped scatterers and antennas.

A current basis function is defined for each non-boundary edge. The RWG basis functions introduced in [9] is used as it is the most appropriate vector basis functions for triangular-patch model. The RWG vector basis function is defined as follows:

$$\mathbf{f}_n(\mathbf{r}) = \begin{cases} \frac{l_n}{2S_{n^+}}\rho_{n^+}, & \mathbf{r} \in P_{n^+} \\ \frac{l_n}{2S_{n^-}}\rho_{n^-}, & \mathbf{r} \in P_{n^-} \\ 0, & \text{otherwise} \end{cases} \quad (6)$$

where l_n is the length of the non-boundary edge number n , S_{n^+} and S_{n^-} are the areas of the triangular patches P_{n^+} and P_{n^-} , respectively. It can be shown that the normal component of $\mathbf{f}_n(\mathbf{r})$ at the n th edge is unity [9]. Using the basis function $\mathbf{f}_n(\mathbf{r})$, the linear current density on the conducting surface can be expressed as

$$\mathbf{J} = \sum_{i=1}^N I_i \mathbf{f}_i \quad (7)$$

where, \mathbf{f}_i is the i th basis function and I_i is unknown amplitude of the basis function associated with non-boundary edge i , and N is the total number of non-boundary edges of the triangular patches constituting the surface S . Now, the same expansion function RWG is used for the testing procedure of Equation (5). After substituting $\mathbf{A}(\mathbf{r})$ and $\Phi(\mathbf{r})$

from Equations (2) and (3), (5) now has the form,

$$\mathbf{E}^i = F(\mathbf{J}) \quad (8)$$

$F(\mathbf{J})$ means that the incident electric field is a function in the induced surface current \mathbf{J} . A set of N linearly independent testing functions \mathbf{f}_i are used. An inner product of each testing function is formed with both sides of the equation being solved. In the case of the EFIE (8), the inner product results in a set of N independent equations of the form,

$$\langle \mathbf{f}_i, \mathbf{E}^i \rangle = \langle \mathbf{f}_i, F(\mathbf{J}) \rangle, \quad i = 1, 2, \dots, N \quad (9)$$

By expanding \mathbf{J} using (2), we obtain a set of N equations in N unknowns,

$$\langle \mathbf{f}_i, \mathbf{E}^i \rangle = \sum_{j=1}^N \langle \mathbf{f}_i, F(I_j, \mathbf{f}_j) \rangle, \quad i = 1, 2, \dots, N \quad (10)$$

This can be written in matrix form as,

$$[V_i] = [Z_{ij}][I_i] \quad (11)$$

where

$$Z_{ij} = \langle \mathbf{f}_i, F(I_j, \mathbf{f}_j) \rangle \quad (12)$$

$$V_i = \langle \mathbf{f}_i, \mathbf{E}^i \rangle \quad (13)$$

and I_j are the unknown amplitudes of the basis functions. The linear system of Equation (10) can, now, be solved to get the unknown current distribution. The involved integrals of (11) are evaluated as in [10].

The scattered electric field, E^s , in the far zone can be evaluated using (1), however, the second term in the right hand side of (1) can be neglected and, hence, the following formula is enough for calculating the scattered field in the far zone,

$$\mathbf{E}^s = -j\omega\mathbf{A} \quad (14)$$

and the RCS can be calculated as [13],

$$\begin{aligned} \text{RCS} &= \frac{\text{backscattered power in the direction of the radar}}{\text{power density of the incident plane wave}} \\ &= 4\pi r^2 \frac{|E_\xi^s|^2}{|E_o|^2} \end{aligned} \quad (15)$$

where E_ξ^s is the scattered field in the ξ direction (direction of the incident electric field, in our case it is the x -direction), E_o is the amplitude of the incident electric field, and r is the distance between the FSS and the far field point.

3. RESULTS AND DISCUSSION

This section presents the results of a free standing planar FSS constructed up as a square array of strip dipole elements. The following discussions are concerned with investigating the characteristics of such an FSS when used as a spatial filter for a reasonably wideband antenna. When the bowtie is used as a transmitter, the transmitted field through the FSS $|E_\theta|$ at a distance 10 m is calculated in the frequency band 4–16 GHz. The bowtie is then used as a receiver antenna, a plane wave source is applied and the received voltage (induced voltage at the input port of the bowtie) is calculated in the same frequency band. The array size of the FSS is reduced to 10×10 elements and the resulting effects on the FSS characteristics are investigated. The effect of interleaving the array elements (sliding the odd columns relative to the even ones) on the frequency response of the FSS is illustrated. The effects of the element size and the spacing between elements on the location of the center frequency of the stop band of the spatial filter are shown. Finally, the effect of the FSS on the radiation pattern of the bowtie is studied at different frequencies.

3.1. Current Distribution on the Elements of a Free Standing Planar FSS

A rectangular array of x -oriented conducting strip dipoles is used to construct the free standing planar FSS as shown in Figure 2. The spacings between elements in x and y direction are dx and dy respectively. The strip dipoles are assumed to be very thin, each dipole is divided into 4 triangular patches with 3 non-boundary edges as shown in Figure 3. The spatial filter is subjected to a plane wave, whose electric field is expressed as,

$$\bar{\mathbf{E}} = (E_x \hat{\mathbf{x}} + E_y \hat{\mathbf{y}} + E_z \hat{\mathbf{z}}) e^{j\bar{\mathbf{k}} \cdot \bar{\mathbf{r}}} \quad (16)$$

where

$$E_x = E_o \cos \theta_i \cos \phi_i \cos \psi_i - \sin \phi_i \sin \psi_i \quad (17)$$

$$E_y = E_o \cos \theta_i \sin \phi_i \cos \psi_i + \cos \phi_i \sin \psi_i \quad (18)$$

$$E_z = E_o \sin \theta_i \cos \psi_i \quad (19)$$

where the angles θ_i and ϕ_i determines the direction of incidence and the angle ψ_i is the polarization angle, which determines the orientation of the electric field.

For a spatial filter constructed as a 25×25 dipole elements, the currents on the dipoles are calculated using the method explained in

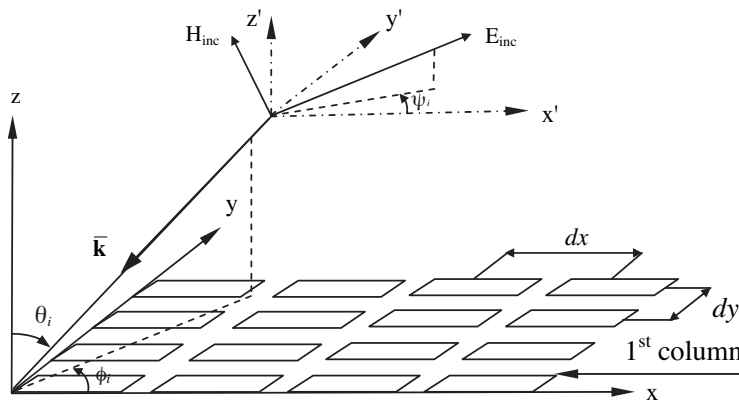


Figure 2. Free standing finite array of conducting dipoles.

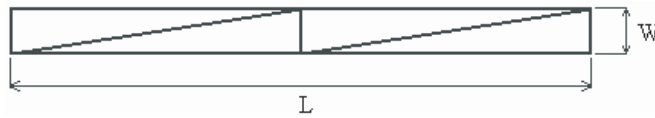


Figure 3. Triangular patch model of the dipole.

Section 2, the real and imaginary parts of the current on the middle row for each element are plotted in Figure 4(a) and Figure 4(b) respectively for 10 GHz frequency. These current distributions are compared to those published in [11], showing good agreement. It is worth mentioning that the values of the currents obtained in this work are exact values as they are calculated for the actual size of the array, but those obtained in [11] are approximate values that depend on the truncation of the infinite summations of the matrix representing the FSS.

3.2. Back Scattering from the Free Standing Planar Spatial Filter

The backscattered field ($|E_{\phi}|$) is calculated and plotted in Figure 5 as a function of the incidence angle θ_i for the planar FSS described in Section 3.1, with the electric field polarized in the direction of the dipoles ($\psi_i = 90^\circ$) and $\phi_i = 90^\circ$ at frequency 8.5 GHz. The results are also compared to those published in [11] showing good agreement. It is worth noting that the maximum backscattered is obtained at $\theta_i = 0^\circ$ and that the field is rapidly reduced with increasing θ_i .

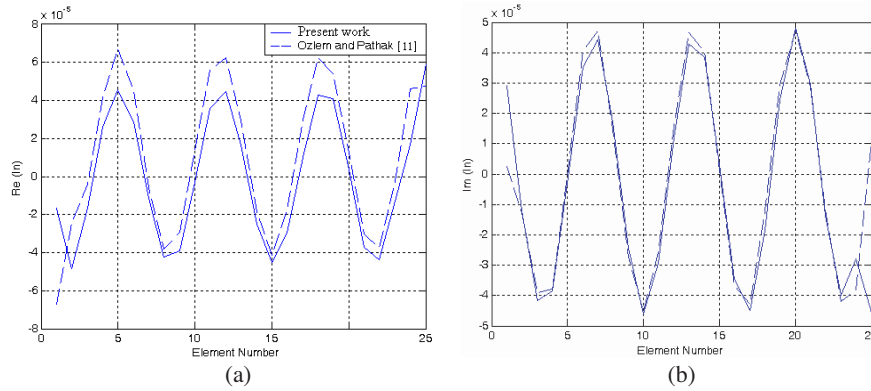


Figure 4. Currents in the elements of the middle column of 25×25 dipole array in free space with $dx = 1.6$ cm, $dy = 0.9$ cm, $L = 1.5$ cm, $W = 0.045$ cm, for horizontally polarized plane wave with $\theta_i = 45^\circ$, $\phi_i = 45^\circ$, $\psi_i = 90^\circ$ and $f = 10$ GHz. (a) real part, (b) imaginary part.

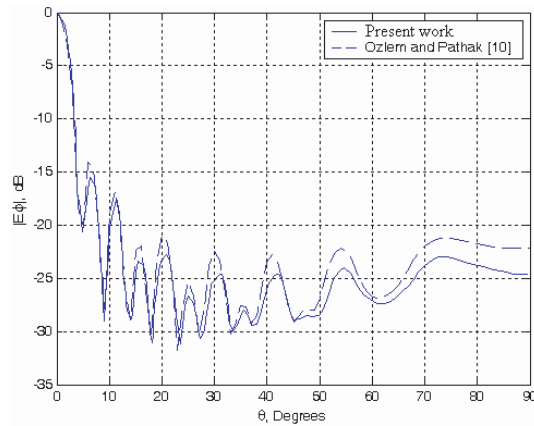


Figure 5. Backscattered from 25×25 dipole array in freespace as a function of θ_i with $dx = 1.6$ cm, $dy = 0.9$ cm, $L = 1.5$ cm, $W = 0.045$ cm, $\phi_i = 90^\circ$, $\psi_i = 90^\circ$, $f = 8.5$ GHz.

3.2.1. Effect of the Polarization of the Incident Electric Field on the Backscattered Field

The effect of the polarization angle ψ_i on the backscattered electric field is studied for normally incident plane wave, $\theta_i = 0$ and $\phi_i = 0^\circ$, at a frequency of 10 GHz. The backscattered electric field component $|E_\theta|$ is

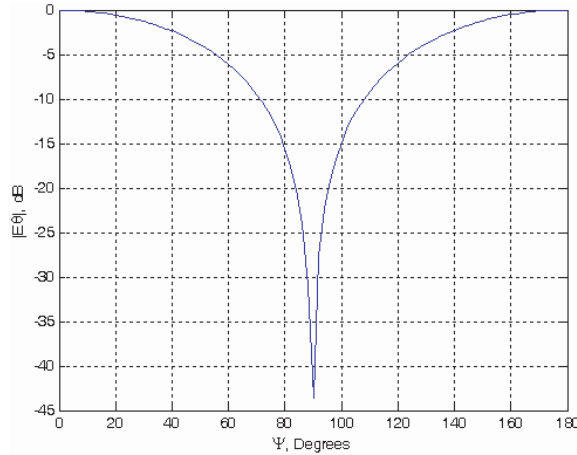


Figure 6. Backscattered field from 25×25 dipole array in free space as a function of the polarization angle ψ_i , with $\theta_i = 0$ and $\phi_i = 0^\circ$, $dx = 1.6$ cm, $dy = 0.9$ cm, $L = 1.5$ cm, $W = 0.045$ cm, $f = 10$ GHz.

plotted versus ψ_i as shown in Figure 6(a). It is clear that the maximum electric field is obtained with $\psi_i = 0^\circ$ and $\psi_i = 180^\circ$ (i.e., the incident electric field is parallel to the axis of the dipoles). This is because the maximum induced current is obtained in this case of polarization. Also it is clear from the figure that $|E_\theta|$ decreases as ψ_i changes farther from 0° , or 180° , till it reaches its minimum value when the incident electric field is perpendicular to the dipole axis ($\psi_i = 90^\circ$), the orientation of the electric field for which the excited electric currents on the dipole elements are almost zero.

3.2.2. Radar Cross Section of the Planar Spatial Filter

The frequency response of the freestanding array of dipoles is studied for the case of normal incident plane wave $\theta_i = 0^\circ$ and $\phi_i = 0^\circ$ with horizontal polarization $\psi_i = 0^\circ$. The radar cross section (RCS) at a point 10 m away from the FSS is calculated over the frequency range from 4 to 17.8 GHz. Figure 7 shows the RCS versus frequency, it is obvious from the figure that the peak of the RCS is at about 11 GHz.

3.3. Operation of the Free Standing Planar FSS as a Band Stop Filter

The planar FSS composed of 25×25 dipole elements with $L = 1.5$ cm and $W = 0.045$ cm, and interelement spacing $dx = 1.6$ cm and

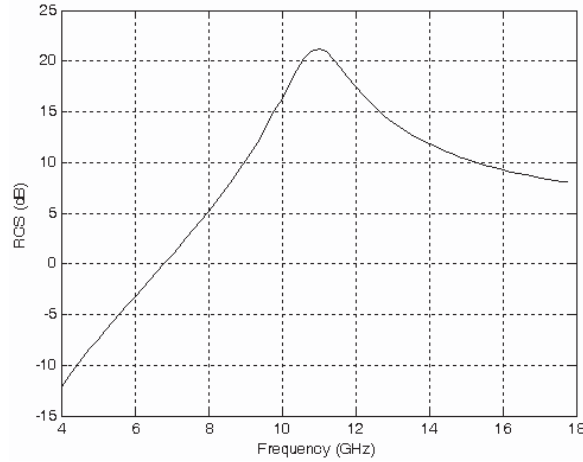


Figure 7. The dependence of the RCS on frequency for 25×25 dipole array in freespace for a horizontal polarized plane wave with $\theta_i = 0^\circ$, $\phi_i = 0^\circ$ and $\psi_i = 0^\circ$ with $dx = 1.6$ cm, $dy = 0.9$ cm, $L = 1.5$ cm, and $W = 0.045$ cm.

$dy = 0.9$ cm, is now used as a radiation filter for a bowtie antenna. The filter characteristics are investigated when the bowtie is used as a transmitter, and also when used as a receiver.

3.3.1. Input Impedance and VSWR of Bowtie Antenna in the Presence of the Planar Spatial Filter

The effects of placing the planar FSS near a bowtie antenna on the antenna input impedance and VSWR are investigated. Figure 8 shows a triangular-patch model for a bowtie antenna. The antenna length is 21.6 mm and the flare angle is 90° . The neck width of the antenna (length of the excitation edge) is 1.08 mm. The triangular-patch model of this antenna has 70 patches and 89 non-boundary edges. This bowtie is a scaled version of that proposed in [12].

The FSS is placed in the xz -plane at $y = 0$, with the dipoles arranged along the z -axis. The bowtie is placed at a distance $R = 3.44$ cm from the spatial filter and takes the same orientation of the dipole elements of the FSS as shown in Figure 9. The dependence of the input impedance of the bowtie antenna on frequency is shown in Figure 10(a) for two cases, a bowtie in free space and a bowtie near the spatial filter. It should be noted that the antenna of the given dimensions is resonant at about 9 GHz where the input impedance is pure resistive. The VSWR of this antenna is also plotted against

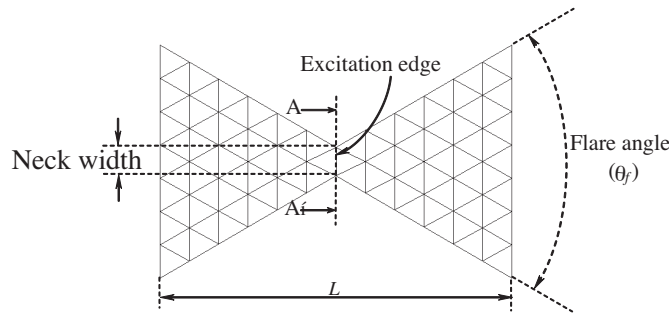


Figure 8. Triangular patch model of a bow-tie antenna.

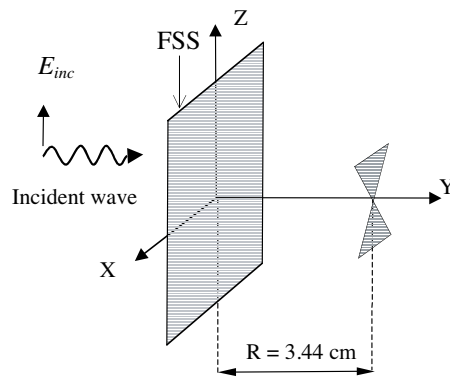


Figure 9. The bowtie is placed behind the planar FSS at a distance $R = 3.44$ cm.

frequency as shown in Figure 10(b) for the two cases, where the source impedance is assumed $300\ \Omega$. It is deduced from the figure that the bandwidth of the bowtie antenna can be considered 4.5 GHz around its resonant frequency, i.e., about 50%. It is clear that the input impedance is stable over a very wide range of frequency. It is clear from Figure 10 that the input impedance and the VSWR of the bowtie are slightly affected by the presence of the FSS.

3.3.2. Bowtie Antenna as a Transmitter

The bowtie antenna described in Section 3.3.1 is used as a transmitter. A delta-gap generator of unity voltage [12] is applied across the cut A-A', i.e., across the non-boundary edge at the center of the antenna. The transmitted field through the FSS $|E_\theta|$ is calculated at $\theta_i = 90^\circ$ and $\phi_i = 270^\circ$ in the frequency range 4–16 GHz and plotted in Figure 11.

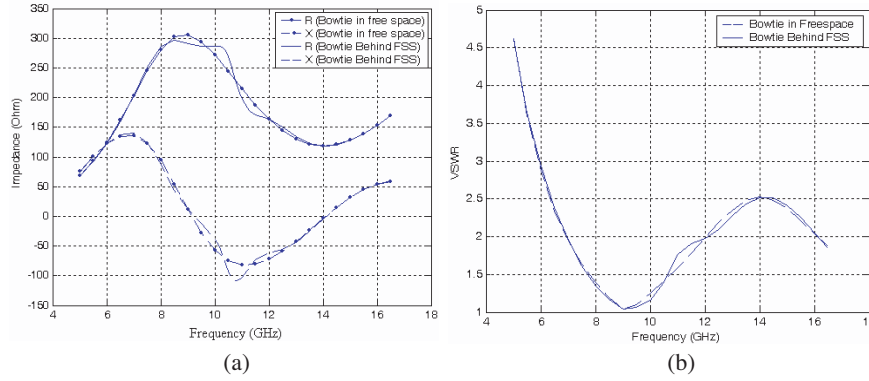


Figure 10. Comparison between input impedance and VSWR of a bowtie antenna in free space and in the presence of a 25×25 planar FSS, bowtie length $L = 21.6$ mm, Neck width = 1.08 mm and $\theta_f = 90^\circ$. (a) input impedance, (b) VSWR.

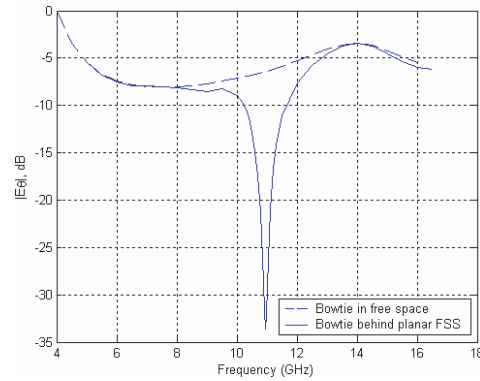


Figure 11. Radiated field ($|E_\theta|$) versus frequency at $\theta_i = 90^\circ$ and $\phi_i = 270^\circ$ for a z -directed bowtie ($L = 21.6$ mm, flare angle = 90° , Neck width = 1.08 mm) located at a distance $R = 3.44$ cm from the 25×25 dipole elements planar FSS.

As shown in the figure, such a planar FSS can operate as a stop band spatial filter with 11 GHz center frequency.

3.3.3. Bowtie Antenna as a Receiver

The bowtie is used as a receiving antenna and the FSS is subjected to a normally incident plane wave with the electric field polarized in the z -

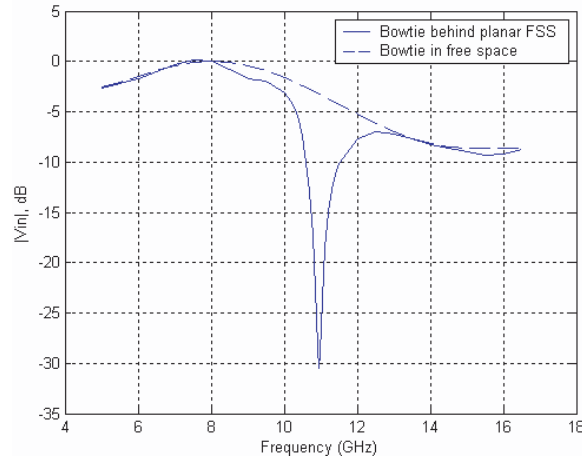


Figure 12. Induced voltage at the input port of the bowtie vs. frequency for a normally incident plane wave on the 25×25 dipole elements planar FSS with z -polarized electric field.

direction. The induced voltage $|V_{in}|$ at the input port of the bowtie is calculated in the frequency range 5–16.5 GHz. The result is compared to the induced voltage in the input port of the bowtie when put in free space with no FSS, the comparison is illustrated in Figure 12. One can deduce from the figure that the FSS has a stop band centered at 10.95 GHz. It may be worth noting that an alternative method to study the characteristics of such a spatial filter is to evaluate the near field just behind the planar FSS using the method described in [14] instead of using a receiving antenna.

3.4. Effect of Reducing the Array Size of the Spatial Filter on Its Performance

In the following discussions, the effect of the FSS array size on the characteristics of the spatial filter is investigated. The array size is reduced to 10×10 elements and the frequency response is studied, when the bowtie is used as a transmitter and when it is used as a receiver. The radiated $|E_{\theta}|$ when the bowtie is a transmitter is shown in Figure 13. The induced input voltage on the input port of the bowtie for a normally incident plane wave with z -polarized electric field, is shown in Figure 14. It is clear from the two figures that reducing the size of the array will still make it exhibit the same characteristics as that of the large one, except for a slight change in the center frequency

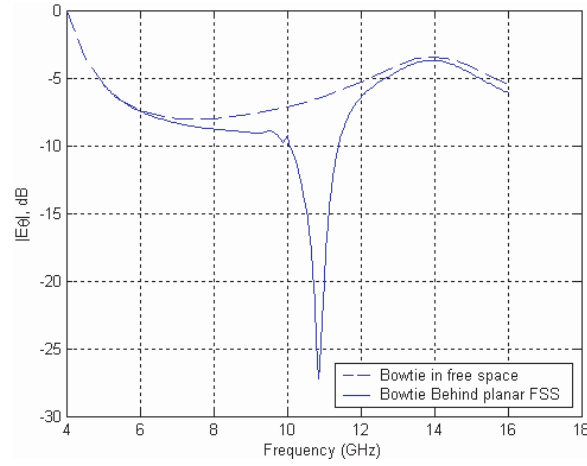


Figure 13. Transmitted field $|E_\theta|$ at $\theta_i = 90^\circ$ and $\phi_i = 270^\circ$ when the bowtie is used as a transmitter, for a 10×10 dipole array, the bowtie is put at a distance $R = 3.44$ cm from the spatial filter.

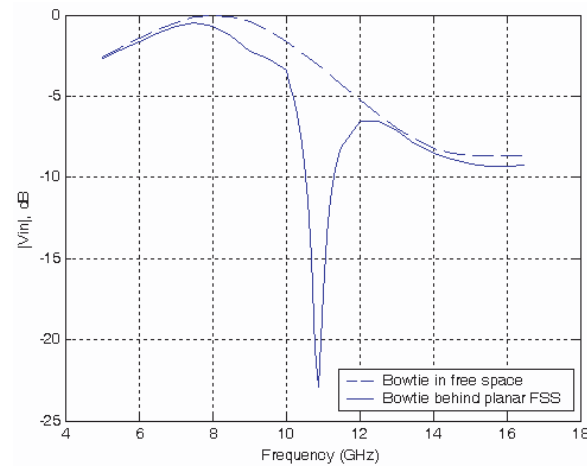


Figure 14. Induced voltage at the input port of the bowtie when used as a receiver, for a 10×10 dipole array, the bowtie is put at a distance $R = 3.44$ cm from the spatial filter.

from 10.95 GHz for the 25×25 dipole array to 10.85 GHz for the 10×10 dipole array. This may be useful in some applications and also useful in reducing the computer resources needed for simulation.

3.5. Frequency Response of a Free Standing Planar FSS with Interleaved Columns

The dipole elements composing the free standing planar FSS can be arranged in a different configuration but still preserving the frequency response of the original FSS. A spatial filter with its even columns shifted a fraction of length (S) with respect to the odd columns, as shown in Figure 15, is one configuration. The dipole length is 1.5 cm and width 0.045 cm, and the spacings between elements are $dx = 1.6$ cm and $dy = 0.9$ cm in the x and y directions respectively. The FSS is put in front of the bowtie antenna at a distance $R = 3.44$ cm. The bowtie antenna has the same dimensions as that described in Section 3.3.1 and is excited with a delta gap generator at the middle edge of the triangular batch model shown in Figure 8. A comparison between the frequency response of the spatial filter with interleaved columns and that of the original one is shown in Figure 5 for different values of S . The radiated field $|E_\theta|$ is plotted over the frequency range 5–16.5 GHz. The results are compared with the values of $|E_\theta|$ for the bowtie antenna in free space. As shown in Figure 5, interleaving the array columns has almost no effect on the frequency response of the far field $|E_\theta|$ radiated from a bowtie antenna placed the spatial filter.

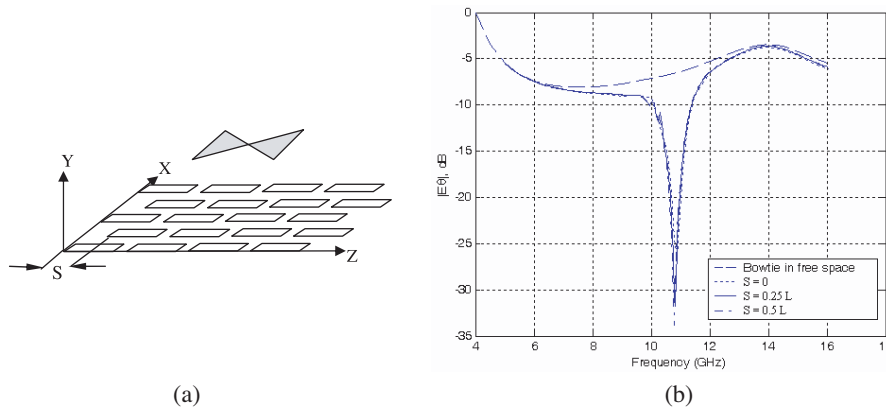


Figure 15. (a) Shifted array FSS, (b) Transmitted $|E_\theta|$ versus frequency at $\theta_i = 90^\circ$ and $\phi_i = 270^\circ$ for the z -directed bowtie located at a distance $R = 3.44$ cm from the 10×10 dipole elements planar FSS for different columns shift (S).

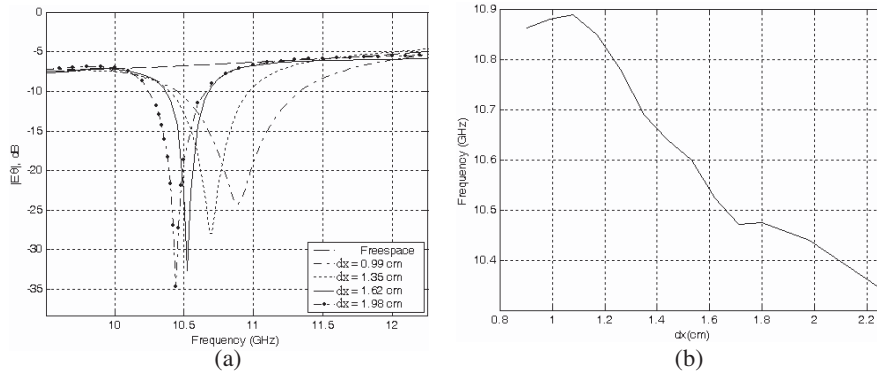


Figure 16. (a) Frequency response for a 10×10 dipole elements FSS with dipole length = 1.5 cm and width = 0.045 for different values of dx , (b) Dependence of the center frequency of the stop band with increasing dx .

3.6. Effect of Changing Spacings between Elements on the Frequency Response of the Spatial Filter

The effect of changing the spacings between elements on the location of the center frequency of the stop band is investigated. The FSS is placed in the xz -plane at $y = 0$, with the bowtie used as a transmitter and placed at a distance 3.44 cm from the FSS. The dipole length = 1.5 cm and width = 0.045 cm. Figure 16(a) shows the frequency response of a 10×10 dipole elements spatial filter for different values of the spacing taking into consideration that dz is increased by the same ratio. Figure 16(b) shows the center frequency of the stop band versus dx . As shown in the figure, the center frequency has a linear dependence on the interelement spacing within ranges.

3.7. Effect of Changing Element Size on the Frequency Response of the Spatial Filter

The effect of the element size on the center frequency of the stop band is illustrated for different element sizes, with $dx = 1.17$ cm and $dz = 2.08$. A bowtie antenna is placed in front of a 10×10 elements FSS at a distance $R = 3.44$ cm and excited with a delta gap generator. The radiated $|E_{\theta}|$ is calculated at a point 10 m apart from the FSS at $\theta_i = 90^\circ$ and $\phi_i = 270^\circ$. Figure 17(a) shows the frequency response of the array with different dipole lengths. The dependence of the center frequency of the stop band on the element size is shown in Figure 17(b). It is clear in the figure that they have linear dependence. It can be

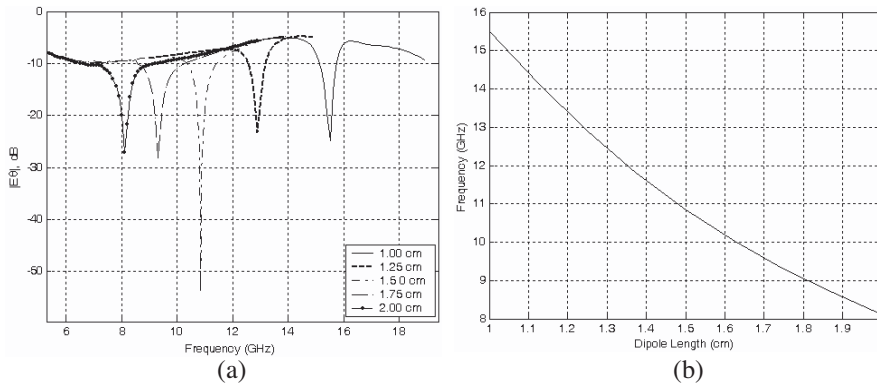


Figure 17. Frequency response for a 10×10 dipole array with $dx = 1.17$ cm and $dz = 2.08$ cm for different element sizes, (b) Dependence of the center frequency of the stop band on the element size.

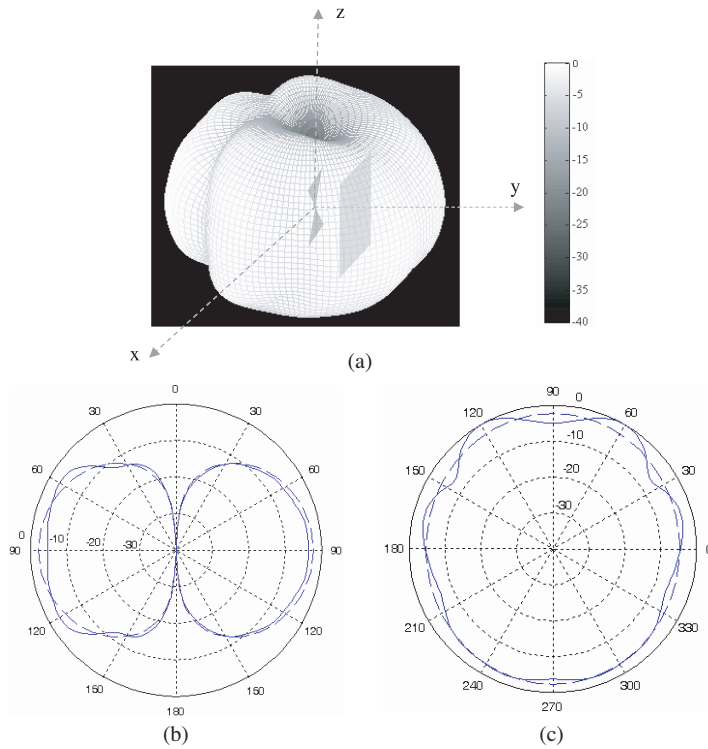


Figure 18. Radiation pattern for bowtie behind a 10×10 dipoles planar FSS placed at 3.44 cm apart from it at $f = 9$ GHz, (a) 3D plot, (b) Elevation plane, (c) Azimuth plane.

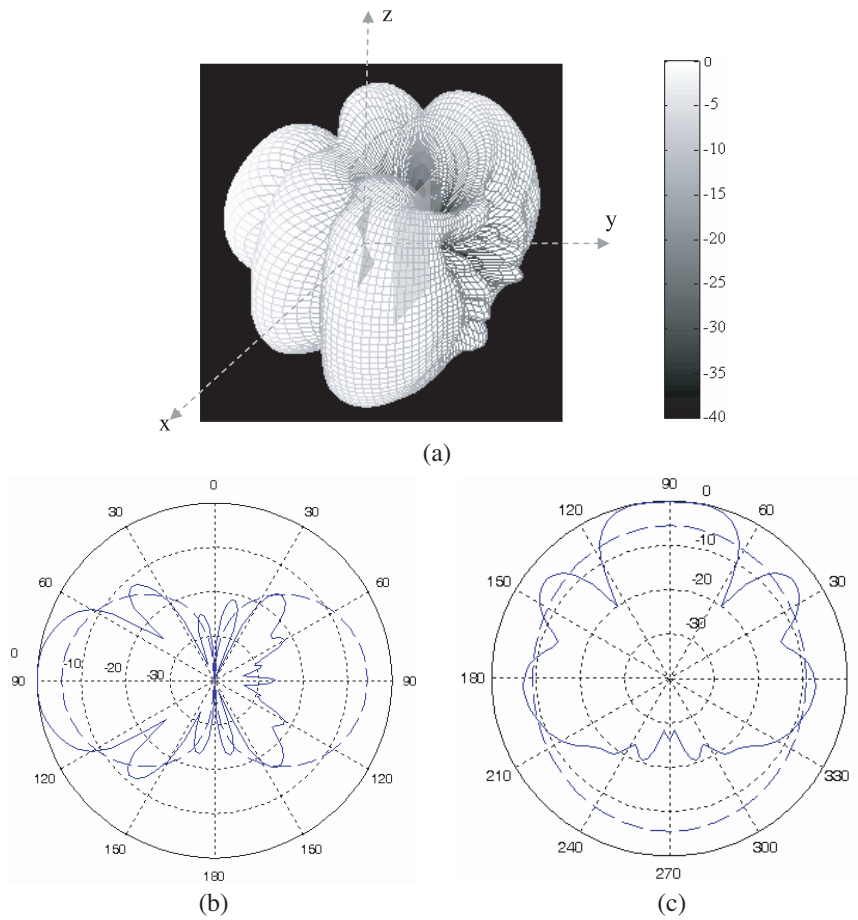


Figure 19. Radiation pattern for bowtie behind a 10×10 dipoles planar FSS placed at 3.44 cm apart from it at $f = 10.85$ GHz, (a) 3D plot, (b) Elevation plane, (c) Azimuth plane.

deduced from Figure 17 that the element size can be used to locate the center frequency of the stop band at certain frequency.

It is clear from Figure 19 that the magnitude of the radiated field is reduced (about 20 dB from the free space value) between $\theta = 60^\circ$ and $\theta = 120^\circ$ in the direction of the spatial filter (i.e., $\phi = 270^\circ$). By noting Figures 19 and 20, it can be seen that the radiation pattern is not much affected by the presence of the FSS as the 9 and 12 GHz are not within the stop band of the FSS.

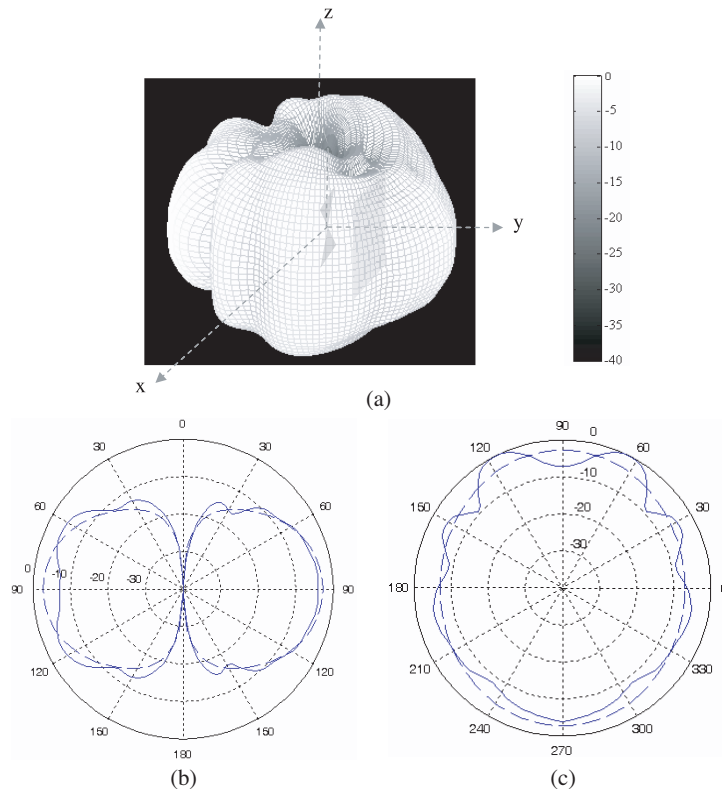


Figure 20. Radiation pattern for bowtie behind a 10×10 planar FSS placed at 3.44 cm apart from it at $f = 12$ GHz, (a) 3D plot, (b) Elevation plane, (c) Azimuth plane.

3.8. Radiation Patterns of a Bowtie Antenna in the Presence of the Spatial Filter

The effect of placing a spatial filter in front of the bowtie on its radiation pattern is studied at different frequencies. The dipole size used here has length of 1.5 cm and width of 0.045 cm, with interelement spacing 0.9 cm and 1.6 cm in x and z -direction respectively. The selected frequencies are chosen as: one frequency before the stop band, another at the center frequency of the stop band, and another frequency after the stop band, those frequencies are 9, 10.85, and 12 GHz respectively. Figure 18(a) shows the 3D plot of the radiation pattern at 9 GHz and Figures 18(b) and 18(c) shows the elevation and azimuth plots also at 9 GHz. Figures 19 and 20 shows the same data for 10.85 GHz and 12 GHz respectively.

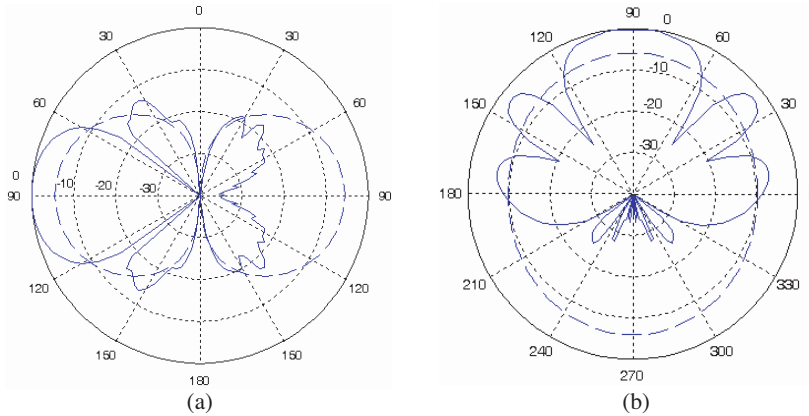


Figure 21. Radiation pattern for a 25×25 dipoles planar FSS at $f = 10.95$ GHz, (a) Elevation plane, (b) Azimuth plane.

The radiation pattern is also plotted at the center frequency of the stop band of the 25×25 dipole elements spatial filter, namely at 10.95 GHz, the results are shown in Figure 21. By comparing this figure with Figure 19, it can be seen that there is much reduction in the magnitude of the radiated field than the 10×10 case, this is because the filter characteristics will improve by increasing the size of the array. This is a design parameter that should be specified by the application requirements.

It should be mentioned here that if we want to reduce the radiated field in all directions around the antenna, we have to use an FSS that surround or enclose the antenna.

4. CONCLUSIONS

In this paper the characteristics of a single layer free standing finite FSSs utilized as spatial filter for linearly polarized antennas, are studied using MoM solution of the EFIE with triangular basis functions used for current expansion on conducting surfaces. From the results, it is evident that arranging the 25×25 array of dipoles with dimensions of 1.5 cm in length and 0.045 cm width for each dipole, and spacings between elements of 1.6 cm in the longitudinal direction (direction of the dipole axis) and 0.9 in the transverse direction will characterize the FSS with a stop band centered at 10.95 GHz. It is also noted that in order to induce the maximum currents on the dipoles, the incident wave should have electric field polarized in the direction of the dipole axis. The proposed FSS is then used as a spatial filter for a bowtie

antenna. The input impedance and VSWR of the bowtie are calculated in free space and in the presence of the spatial filter. It is found that placing the FSS in the vicinity of the antenna will have a negligible effect on its impedance and VSWR. The effect of reducing the size of the array is investigated and it is found that a reduced array of 10×10 elements will exhibit the same characteristics as the 25×25 dipoles array. Also, it is exploited that interleaving the array columns will not alter the array characteristics. The effect of changing element size and interelement spacing are studied. It is found that they can help locate the center frequency of the stop band at certain frequency. It is shown from the radiation pattern for the bowtie that radiation intensity is much reduced at the direction of the FSS. Thus, the proposed FSS can be used as radiation filter for linearly polarized antennas.

REFERENCES

1. Agrawal, V. D. and W. A. Immbriale, "Design of a dichroic Cassegrain subreflector," *IEEE Trans. Antennas Propagat.*, Vol. 27, No. 4, 466–473, Jul. 1979.
2. Lee, S.-W., "Scattering by dielectric loaded screen," *IEEE Trans. Antennas Propagat.*, Vol. 19, No. 5, 656–665, Sept. 1971.
3. Hirai, J. and I. Yokota, "Electromagnetic shielding glass of frequency selective surfaces," *Electromagnetic Compatibility International Symposium*, 314–316, 1999.
4. Unal, E., A. Gokcen, and Y. Kutlu, "Effective electromagnetic shielding," *IEEE Microwave Magazine*, Vol. 7, No. 4, 48–54, Aug. 2006.
5. Govindaswamy, S., J. East, F. Terry, E. Topsakal, J. L. Volakis, and G. I. Haddadm, "Frequency selective surface based band pass filters in the near infrared region," *Microwave and Optical Technology Letters*, Vol. 41, No. 4, May 2004.
6. Qing, A., "Vector spectral-domain method for the analysis of frequency selective surfaces," *Progress In Electromagnetics Research*, PIER 65, 201–232, 2006.
7. Vardaxoglou, J. C., *Frequency Selective Surface, Analysis and Design*, Research Studies Press Ltd., Taunton, England, 1997.
8. Chen, C. C., "Scattering by a two dimensional periodic array of conducting plates," *IEEE Trans. Antennas Propagat.*, Vol. 18, 660–665, 1970.
9. Rao, S. M., D. R. Wilton, and A. W. Glisson, "Electromagnetic scattering by surfaces of arbitrary shape," *IEEE Trans. Antennas Propagat.*, Vol. 30, 409–418, May 1982.

10. Hussein, K. A., "Fast computational algorithm for EFIE applied to arbitrarily shaped conducting surface," *Progress In Electromagnetics Research*, PIER 68, 339–357, 2007.
11. Özlem, A. C. and P. H. Pathak, "Array guided surface waves on a finite planar array of dipoles with or without a grounded substrate," *IEEE Trans. Antennas Propagat.*, Vol. 54, No. 8, 2244–252, Aug. 2006.
12. Hussein, K. F. A., "Accurate computational algorithm for calculation of input impedance of antennas of arbitrary shaped conducting surfaces," *Applied Computational Electromagnetic Society Journal*, Vol. 22, No. 3, Nov. 2007.
13. Hussein, K. A., "Effect of internal resonance on the radar cross section and shield effectiveness of open spherical enclosures," *Progress In Electromagnetics Research*, PIER 70, 225–246, 2007.
14. Hussein, K. A., "Efficient near-field computation for radiation and scattering from conducting surfaces of arbitrary shape," *Progress In Electromagnetics Research*, PIER 69, 267–285, 2007.
15. Yuan, N., X.-C. Nie, Y.-B. Gan, T.-S. Yeo and L.-W. Li, "Accurate analysis of conformal antenna arrays with finite and curved frequency selective surfaces," *Journal of Electromagnetic Waves and Applications*, Vol. 21, No. 13, 1745–1760, 2007.
16. Li, D., Y. J. Xie, P. Wang, and R. Yang, "Applications of split-ring resonances on multi-band frequency selective surfaces," *Journal of Electromagnetic Waves and Applications*, Vol. 21, No. 11, 1551–1563, 2007.
17. Ma, D. and W. X. Zhang, "Mechanically tunable frequency selective surface with square-loop-slot elements," *Journal of Electromagnetic Waves and Applications*, Vol. 21, No. 15, 2267–2276, 2007.
18. Oraizi, H. and M. Afsahi, "Analysis of planar dielectric multilayers as FSS by transmission line transfer matrix method (TLTMM)," *Progress In Electromagnetics Research*, PIER 74, 217–240, 2007.
19. Pirhadi, A., F. Keshmiri, M. Hakkak, and M. Tayarani, "Analysis and design of dual band high directive EBG resonator antenna using square loop FSS as superstrate layer," *Progress In Electromagnetics Research*, PIER 70, 1–20, 2007.
20. Delihacioglu, K., S. Uckun, and T. Ege, "FSS comprised of one- and two-turn square spiral shaped conductors on dielectric slab," *Progress In Electromagnetics Research B*, Vol. 6, 81–92, 2008.